VOL. 16, NO. 13, JULY 2021 ISSN 1819-6608
ARPN Journal of Engineering and Applied Sciences

www.arpnjournals.com

NUMERICAL SIMULATION OF FORCED CONVECTIVE FLOWS OVER A PAIR OF SIDE-BY-SIDE HEATED CIRCULAR CYLINDERS

O. M. Oyewola[1], P. M. Singh[1], O. S. Ismail[2] and K. Abu[2]
[1]School of Mechanical Engineering, Fiji National University, Suva, Fiji
[2]Department of Mechanical Engineering, University of Ibadan, Ibadan, Nigeria
E-Mail: oooyewola001@gmail.com

ABSTRACT

This study examines the forced convective incompressible flow over a pair of side-by-side equal-sized circular cylinders confined in a rectangular channel in order to examine the influence of spacing on the heat transfer characteristics and the hydrodynamic force coefficients. Air with Prandtl number of 0.702 flows through the inlet at free stream temperature and velocity of T_∞ (=25ºC) and U_∞(= 4.139m/s) respectively over the cylinders. The cylinder walls are at temperature T_w, where $T_w > T_\infty$. The numerical study is carried out by solving continuity, momentum and energy equations using finite-element based software (COMSOL Multiphysics) at $Re_D = 2.35 \times 10^4$ and S/D = 1.1, 1.3, 2.0, 2.4, 3.0, 4.0 and 5.0. The results show that the drag and lift coefficients as well as the wake interactions depend strongly on spacing ratio. Biased flip-flop and anti-phase synchronised patterns were observed for the lift coefficients at S/D =2 and 3 respectively. At small spacing ratios S/D ≤ 2, there is strong wake interaction between the cylinders whereas for S/D > 4, vortex structure interaction between the cylinders vanishes. Mean Nusselt numbers on the front, top, rear and bottom parts of the two cylinders are found to decrease as the S/D ratio increases. For all S/D, there are more isotherm contours on the front part than any other portions of the cylinders. This implies that the greatest heat transfer occurs on the front parts of the cylinders, and thereby flow interference on side-by-side structures is minimised at S/D > 2.

Keywords: mean nusselt number, drag coefficient, lift coefficient, side by side, forced convection.

1. INTRODUCTION

Flow over cylinders has been studied for more than four decades mainly because of its practical applications. For instance, Zdravkovich [1] summed up the significance of flow interference in practical applications to include chimney stacks in wind and jetties as well as offshore structures in high seas, vibration of two conductor transmission lines, vibration in heat exchanger tubes to mention but a few. Further, considerable works on flow over bodies in order to account for the heat transfer between such structures or components have been a subject of attention. It should be noted that such components are being modelled by bluff bodies like cylinders [2, 3]. Moreover, other than dynamic vibrations applications, the study of two structures in proximity to each other has also been employed in accounting for loss of heat from high-rise buildings, cooling towers, offshore rises, nuclear reactor rods, cooling of electrical components, etc. [4, 5].

In the study of flow over two cylinders, Reynolds number Re and spacing ratio S/D (where S is the distance between the centres of the cylinders, and D is the diameter of the equal-sized cylinders) has been considered as important parameters since they play significant roles in the mutual interaction between the cylinders. For instance, Sarvghad-Moghaddam *et al.* [6] used finite-volume Cartesian based solver to simulate the flow field over two side-by-side cylinders for low Reynolds numbers Re = 100, 200, and 10 000 with spacing ratios S/D = 1.5, 2, 3 and 4. They presented the relationship between the drag coefficient as well as the lift coefficient and the spacing ratios at each of the Reynolds numbers as well as identifying different flow patterns such as biased/bi-stable flow, flip-flopping pattern, symmetric flow, asymmetric flow, and synchronised anti-phase and in-phase flows. Their simulation at Re = 100 is consistent with the result of Kang [7], who used the immersed boundary method to investigate two dimensional flow over two side-by-side equal sized cylinders for Reynolds numbers between 40 and 160 at different S/D less than 5. He identified six flow patterns: anti-phase synchronised, in-phase synchronised, flip-flopping, deflected, single bluff body and steady wake patterns. Chen *et al.* [8] also observed six near-wake patterns for cross-flow over two side-by-side cylinders for Re =100 and S/D ranges from 2 to 5.

The vortex shedding behind the cylinders which depends on Reynolds number may be anti-phase or in-phase. Cases of anti-phase vortex shedding behind the cylinders are predominant at a critical spacing ratio (between 1 and 5) between two bluff bodies [9]. The numerical work of [6] corroborated the experimental findings of [9] which showed that within those critical spacing ratios, there might still occur in-phase vortex shedding and synchronisation behind the cylinders. These various flow patterns are due to fluctuations taking place in the wake of the cylinders. Bearmann and Wadcock [10] showed that base pressures at the cylinders fluctuated between two extremes. They also found that asymmetry was pronounced at spacing ratio between 0.1 and 1. When the cylinders are in very close proximity, they indicated that repulsive force existed between the two cylinders. Meneghini and Saltra [11] also showed in their numerical investigation of flows over side-by-side cylinders at Re = 100 - 200 using fractional step method that a repulsive force acted on the cylinders at spacing ratio of 1.5, which affected the net pressure field. Sumner *et al.* [12] reported that at spacing ratio between 1 and 1.2, gap flow parallel to the flow axis occurred and persisted until spacing ratio

of 2.0. They conducted experimental investigation using the Particle Image Velocimetry (PIV) as well as hot-film anemometry to study the flow field over two and three side by side circular cylinders for Re = 500-3000 at spacing ratios ranging from 1 to 6. They showed that vortex shedding for Re = 1000-3000 is anti-phase at spacing ratios of 2.5 and 4.5. Although, they did not categorically observed bistable nature in their water-tunnel experiment, they suggested that residual motion of the water in the towing tank might be responsible for the flow being deflected towards the same cylinder. They resolved that at spacing ratio greater than 4.5, no form of synchronisation between the cylinders was apparent.

Aside from vortex-induced vibration of cylinders, studies have also been carried out to investigate flow over oscillating cylinders. Bao*et al.* [13] conducted study on flow over two in-phase oscillating cylinders using the Characteristic-based-split finite element method with MINI triangular element at Re = 100 and S/D ranging from 1.2 to 4.0 and excitation frequency ratio in the range of 0.5 and 2.0. They identified lock-on flow state at all gap spacing. At S/D $\geq$ 2.5 their study showed that lock-on state can be observed around frequency ratio approximately unity which corresponded to synchronised vortex shedding flow pattern for the stationary system. They identified altogether pure lock-on response, imperfect lock-on response, quasi-periodic response regime I, quasi-periodic response regime II and periodic doubling response regimes. Lee *et al.* [14] investigated the flow around two out-of-phase oscillating side-by-side cylinders at Re = 185, mean spacing ratio g = 0.6, 1.0, 1.4 and 1.8 and at oscillating frequency ratio f_e/f_o = 0.8, 1.0 and 1.2 using the immersed boundary method, where $f_e$is the excitation frequency of the cylinder, f_o is the natural frequency of one cylinder at Re =185. They reported that for g =1.8, lock-in regime occurred at only f_e/f_o = 1.2. For $0.8 \leq f_e/f_o \leq 1.2$, they identified anti-phase synchronised and deflected patterns for the lift and drag coefficient. Anti-phase synchronised vortices were formed which merged downstream. These patterns in drag and lift coefficients were also observed at g = 1.4 for the same range of frequency ratios. At g =1.0, single bluff-body, flip-flop and anti-phase synchronised patterns were found for $0.8 \leq f_e/f_o \leq 1.2$. At g = 0.6, the lift and drag coefficients were observed to have single bluff-body and deflected patterns for f_e/f_o = 0.8 and 1.0, but were of single bluff-body and flip-flop patterns for f_e/f_o = 1.2. They stated that for all the frequency ratios due to the small gap, single bluff body pattern was observed for vortex shedding.

Beyond induced vibrations due to flow over structures, the heat characteristics of flow over two cylinders have also been investigated. Golani and Dhiman [15] presented simple correlation between time-averaged Nusselt number as a function of Re in their study of flow patterns and heat transfer of flow across an unconfined cylinder at Re ranging from 50 and 180. Yoon *et al.* [16] carried out numerical investigation of convection heat transfer around rotating cylinders using the immersed-boundary method at Re =100 and absolute rotational speed $|\alpha| \leq 2$ and spacing ratios of 3, 1.5, 0.7 and 2.0. They showed that both time and surface-averaged Nusselt numbers decreased as the $|\alpha|$ increased for all the gap ratios. Chaitanya and Dhiman [17] used ANSYS FLUENT to simulate non-Newtonian power-law flow and heat transfer across a pair of side-by-side cylinders at Prandtl number of 50, Re ranging from 1 to 40, S/D ranging from 1.5 to 4.0, power indices of n = 0.4 – 1.8, where n < 1 is shear-thining, n =1 is Newtonian and n > 1 is shear-thickening. They found that total drag coefficient is higher for shear-thinning fluids than Newtonian and shear-thickening fluids at Re $\leq$ 10, whereas the reverse occurred at Re > 10 for all the S/D. The average Nusselt numbers were found higher for shear-thinning fluids than Newtonian and shear-thickening fluids for all Re and S/D. Dos-Santos *et al.* [18] studied transient forced convective turbulent flow (Re=22 000) over a pair of cylinders, considering two arrangements: side-by-side arrangement and the tandem arrangement using FLUENT. The Nusselt number and drag coefficient about the two cylinders were found to be higher for side by side arrangement than for tandem arrangement.

In this paper, parametric study based on spacing ratios are carried out to determine the heat characteristics, drag coefficient and lift coefficient of forced convective flow over a pair of circular cylinders confined in a rectangular channel. It should be noted that various authors [6, 8, 12, 18] as evidenced in literature, have demonstrated that flow-induced vibrations and interferences in the wake of two circular cylinders have great effect on the flow structures especially at low (Re = 100, 200,500) and high Reynolds numbers (Re = 3000, 10000 and 22000). The importance of parameter such as spacing ratio has been noted to play significant role. Sarvghad-Moghaddam *et al.* [6] presented the drag and lift coefficients behind two cylinders at Re = 10 000; they did not examine the phenomenon of heat transfer. While [18] considered the effects of various Nusselt numbers and force coefficients as dependent on the arrangement of two cylinders at Re = 22000, they did not show how spacing could impact their result. Further, [16] examined influence of spacing on convective heat transfer of two rotating cylinders at laminar Reynolds number regime Re =100. Therefore, this present work considers the effect of spacing ratios on both the fluid dynamic force coefficients and heat transfer characteristics over a pair of circular cylinders at high subcritical Reynolds number Re_D= 23 500. The finite-element-method based software (COMSOL Multiphysics) is adopted as against the popular simulation Software ANSYS FLUENT [used by 16 and 17]. COMSOL Multiphysics has not been widely reported to have been used for this area of study, yet it is easy to implement. The influence of spacing ratios on the hydrodynamic force coefficients and heat transfer characteristics across the cylinders at Reynolds number of 23 500 and at S/D = 1.1, 1.3, 2.0, 2.4, 3.0, 4.0 and 5.0 is examined. The motivation for this study is to investigate the conditions similar to those of heat exchanger tubes and high-rise structures in the wake of fluid flow. This work would find applications in heat exchangers and structures

for the optimisation of flow-induced vibrations and heat transfer.

2. PROBLEM DESCRIPTION, PHYSICS AND MODELLING

Air flows into a rectangular channel at free stream temperature T_∞ (25ºC), and free stream velocity U_∞ (4.139m/s). In the channel, two circular cylinders are placed at some points away from the inlet, with equal distance from the centreline of the channel (Figure-1). The two cylinders are heated to surface temperature T_w (70 ºC); the surface temperature is higher than the free stream temperature of the fluid. The bulk temperature of the fluid T_b, which is $(T_w + T_\infty)/2$ is 47.5 ºC. At the bulk temperature the thermo-physical properties such as the dynamic viscosity and the density of dry air are used for calculation of the free-stream velocity. The Prandtl number of air considered is at 25ºC is 0.702. In laminar flow, no-slip condition is specified on a solid surface, where all the velocity components are zero. Laminar flow is characterized with fluid layers moving slowly and smoothly past each other without causing mixing, so that next to a solid surface the fluid layer is at rest. However, in turbulent flow, fluid molecules experience random changes in velocity both in space and time [19]. As a result, the fluid layer next to the solid surface does not have all its velocity components to be zero. Relevant explanation of slip boundary can be found in the work of Yang [26]. In turbulent flow, the tangential force from the flow of the fluid exceeds the intermolecular attraction between a solid surface and the fluid molecules next to it to satisfy slip boundary. However, the normal velocity at the solid cylinder surface/wall is zero [27]. Therefore, the slip wall boundary condition ensures that fluid does not leave the wall domain, i.e. the wall or does not penetrate through the cylinder as specified in Figure-1. The initial temperature through the bulk of the flow domain is assumed to be the same before the cylinders would be heated up. The purpose of heating the cylinders is to investigate the thermal effects around them.

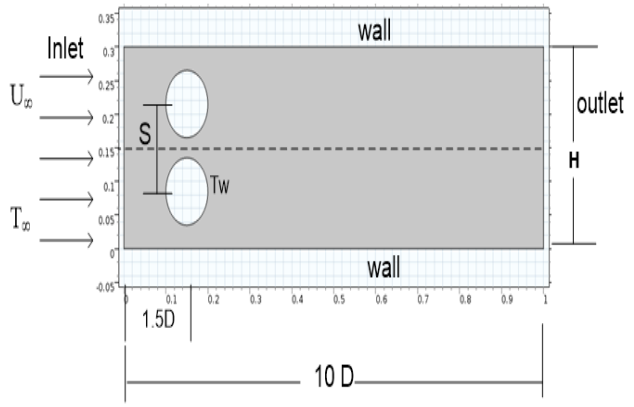

Figure-1. Two cylinders of equal diameter in side-by-side arrangement. H refers to the height of the channel.

The cylinders are placed in the rectangular channel in side-by-side arrangement. Both cylinders are placed (1.5D) away from the inlet. Spacing ratios 1.1, 1.3, 1.5, 2.0, 2.4, 3.0, 3.5, 4.0 and 5.0 are used.

The problem is investigated at the fixed Reynolds number based on diameter of the cylinder (Re_D = 23500). Simulations are carried for the different spacing ratios at this Reynolds number. The effects of the S/D ratios on isotherms, temperature field, average Nusselt number (Nu), vortices, streamlines, drag and lift coefficients around the two cylinders are evaluated.

2.1 Configuration of Fluid Flow Domain

The fluid domain is rectangular. The length of the domain is 10D, while the height is variable to leave space between the top boundary and the upper cylinder as well as between the lower boundary and the lower cylinder. This is to avoid interference with vortex shedding. The cylinders are placed 1.5D downstream, i.e., away from the inlet. For the various spacing used in this arrangement, the dimensions of the rectangular are shown in Table-1.

Table-1. The spacing between the two cylinders arranged side by side.

S/D	Length	Height
1.1	10D	3D
1.3	10D	3D
2.0	10D	3.5D
2.4	10D	3.7D
3.0	10D	4.4D
4.0	10D	5.5D
5.0	10D	8.0D

2.2 Governing Equations and Boundary Conditions

The differential equations that govern unsteady incompressible turbulent flow are given by the continuity and momentum equations as follows [19]

$$\frac{\partial(\overline{v_i})}{\partial x_i} = 0 \qquad (1)$$

$$\frac{\partial(\overline{v_i})}{\partial t} + \frac{\partial(\overline{v_i}\,\overline{v_j})}{\partial x_j} = -\frac{1}{\rho}\frac{\partial \overline{P}}{\partial x_i} + \frac{1}{\rho}\frac{\partial}{\partial x_j}\left((\mu + \mu_t)\frac{\partial \overline{v_i}}{\partial x_j} + \tau_{ij}\right) \qquad (2)$$

$$\tau_{ij} = -\overline{\rho v_i v_j} = 2\mu_t S_{ij} - \frac{2}{3}\overline{\rho} k \delta_{ij}$$

where i = 1, 2; means the Reynolds stress.

$S_{ij} = \frac{1}{2}\left(\frac{\partial \overline{v_i}}{\partial x_j} + \frac{\partial \overline{v_j}}{\partial x_i}\right)$ is strain deformation and k is the turbulent kinetic energy per unit mass. μ_t is the turbulent (eddy) viscosity; μ is molecular dynamic viscosity; and t is time. The overhead bar signifies time-average.

The energy equation is given in Equation (3).

$$\frac{\partial(\overline{T})}{\partial t}+\frac{\partial(\overline{v_i}\,\overline{T})}{\partial x_i}=\frac{\partial}{\partial x_i}\left\{\alpha\frac{\partial\overline{T}}{\partial x_i}+q_i\right\}+q''' \quad (3)$$

where $q_i=-\overline{v_i T}$ is similar to the Reynolds stress, α is thermal diffusivity and q''' is heat generation per unit volume.

The turbulence is modelled using the standard k-ε model [19-20].

$$\frac{\partial(\rho k)}{\partial t}+\nabla\cdot\left(\rho k\vec{V}\right)=\nabla\cdot\left[\frac{\mu_t}{\sigma_k}\nabla k\right]+2\mu_t S_{ij}\cdot S_{ij}-\rho\varepsilon \quad (4)$$

$$\frac{\partial(\rho\varepsilon)}{\partial t}+\nabla\cdot\left(\rho\varepsilon\vec{V}\right)=\nabla\cdot\left[\frac{\mu_t}{\sigma_\varepsilon}\nabla\varepsilon\right]+c_{1\varepsilon}\frac{\varepsilon}{k}2\mu_t S_{ij}\cdot S_{ij}-c_{2\varepsilon}\rho\frac{\varepsilon^2}{k} \quad (5)$$

Turbulence viscosity μ_t is given by $\mu_t=\rho c_\mu\frac{k^2}{\varepsilon}; c_{1\varepsilon}=1.44; c_{2\varepsilon}=1.92;$ $c_\mu=0.09; \sigma_k=1.00; \sigma_\varepsilon=1.30$ are constants and $\vec{V}$ is the velocity vector.

The lift and drag coefficients are evaluated using the following equations [5].

$$C_D=\frac{F_D}{\frac{1}{2}\rho U_\infty^2 D} \quad (6)$$

$$C_L=\frac{F_L}{\frac{1}{2}\rho U_\infty^2 D} \quad (7)$$

The heat transfer over the cylinders is evaluated as follows [21].

$$q''=-K_{fluid}\frac{dT}{dx}_{x=0} \quad (8)$$

$$q''=h_\theta(T_w-T_\infty) \quad (9)$$

$$h_\theta=\frac{-K_{fluid}\frac{dT}{dx}_{x=0}}{(T_w-T_\infty)} \quad (10)$$

In order to measure the convective heat transfer at a solid surface of the cylinder, a dimensionless number called Nusselt number is defined. Based on diameter, Nusselt number is given as follows.

The local Nusselt number is defined as

$$Nu_\theta=\frac{h_\theta D}{K} \quad (11)$$

The boundary conditions adopted for this study are described as follows:

a) Inlet: u= U_∞, T = T_∞. The inlet is 1.5D away from the cylinders

b) Outlet: $\frac{\partial u}{\partial x}=0;\frac{\partial v}{\partial x}=0;\frac{\partial T}{\partial x}=0$, and pressure p=0.

c) The top and bottom walls as well as the cylinder walls use the slip wall boundary condition.

The slip wall boundary condition ensures that fluid does not leave the domain or does not penetrate through the cylinder [22]. It can be applied to both a stationary wall and a moving wall/solid surface [27]. In this work, the cylinders are stationary. The fluid viscosity is not neglected, but at the solid surface or wall, the tangential force provided by the turbulent is assumed to exceed the intermolecular attraction between neighbouring fluid molecules and the solid surface. Consequently, the fluid slips tangentially over this surface/wall, as if it was an inviscid flow in which the shear stress arising from intermolecular attractions between the surface/wall and the near fluid molecules is set to zero [27].

Mathematically, the constrained is defined as:

$$\vec{v}\cdot n=0 \quad (12)$$

$$K-(K.n)n=0 \quad (13)$$

Where

$$K=\mu\left(\nabla\vec{v}+\left(\nabla\vec{v}\right)^T\right)n \quad (14)$$

d) The temperature at the upper and bottom surfaces is T = T_∞, while the cylinder walls temperature are set to T=T_w.

The governing differential equations with the appropriate boundary conditions were solved using finite element method, implemented in COMSOL Multiphysics at Re_D =23500.

2.3 Choice of Numerical Method

Finite element method (FEM) and finite volume method (FVM) are both numerical solution techniques which involve subdividing a geometry into elements and control volumes respectively. FVM integrates the partial differential equation and solves over each control volumes, with fluxes across the connected control volumes ensuring law of conservation of the particular physical property being considered [19]. Though FVM ensures conservation property, it requires more effort to handle irregular geometries. It requires a lot of mathematics- use

of polynomial functions and weighted residuals- and so results in greater computational cost [28]. Based on its ability to handle complex geometries and meshes, though with more computational time and memory [29], this finite element method was adopted for this work.

2.4 Mesh Generation

Mesh generation is the step in numerical simulation with which the set of finite elements are obtained. The geometry is subdivided into non-overlapping finite elements. The equations are then solved for each of the elements in the mesh generated to obtain pressure, velocity and temperature at every node in the computational domain. The sizes of the mesh influences the accuracy of the results obtained.

Mesh sizes, the computer system's memory and the problem complexity altogether determine the solution time. Triangular (some are quadrilateral) elements of finer sizes, compared to coarse meshes, brings about increase in solution time but improves the accuracy of the results. Figure-2a shows a mesh ("finer mesh" type) built for the S/D = 3.5 simulation case, using COMSOL. The mesh has 18607 elements. The problem complexity includes the geometry, the number of cylinders, and the Reynolds number. In this work, normal, fine and finer physics-defined mesh sizes were evaluated over two cylinders at S/D = 3.5. For this S/D = 3.5, the finer mesh uses 18607 elements, fine mesh has 8103 elements and normal mesh has 4243 elements. With normal mesh used, the simulation time was 20 minutes, while the simulation time was 32 minutes for fine mesh (Table-2). However, the simulation time for finer mesh was very high (time is 10 hours) as shown in Table-2, yet the percentage differences in CD and CL between the finer mesh and fine mesh range between 0.7%-1.5%. This shows that the results obtained at fine mesh are independent of the mesh sizes. Therefore, the fine physics-defined mesh, which required less simulation time, was adopted throughout the rest of the work. The solution time for simulation of flow over the heated cylinders at Reynolds number 23500 using the two mesh sizes is summarised in Table-2. Further, with fine mesh adopted, y+ values were determined in relation to the u^+ values for S/D = 3.5. The purpose was to ensure that the mesh quality is sufficient for turbulence modelling. Based on this, Figure-2b captures the outer layer (representing the defect layer/wake law, which is obtained as a trendline) of a boundary layer. The defect layer lies outside of the log law, begins where y+ > 700 [30], with the bulk flow far from wall and not under direct viscous effects [19]. This establishes the suitability of the fine mesh size for the turbulence modelling and vortex shedding behind the cylinders.

Table-2. Mesh statistics by side arrangement at ReD = 23500.

S/D	Normal Mesh		Time (min)	Fine Mesh		Time (min)	Finer Mesh		Time (h)
3.5	CD LC	0.964	20	CD LC	0.851	32	CD LC	0.821	10
	CD UC	0.970		CD UC	0.821		CD UC	0.833	
	CL LC	-0.195		CL LC	-0.111		CL LC	-0.11	
	CL UC	0.056		CL UC	0.0978		CL UC	0.097	

UC refers to the upper cylinder while LC means lower cylinder

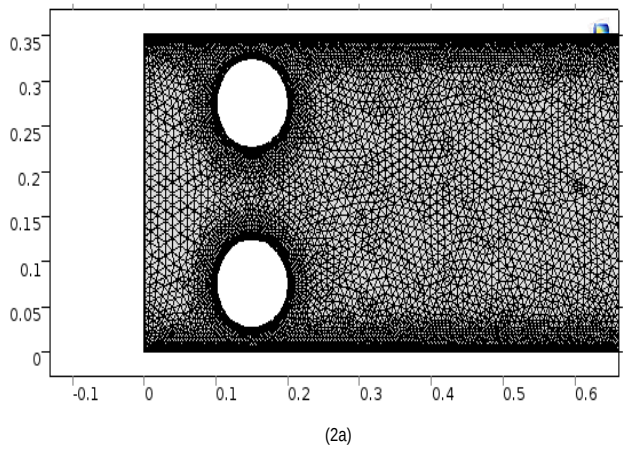

(2a)

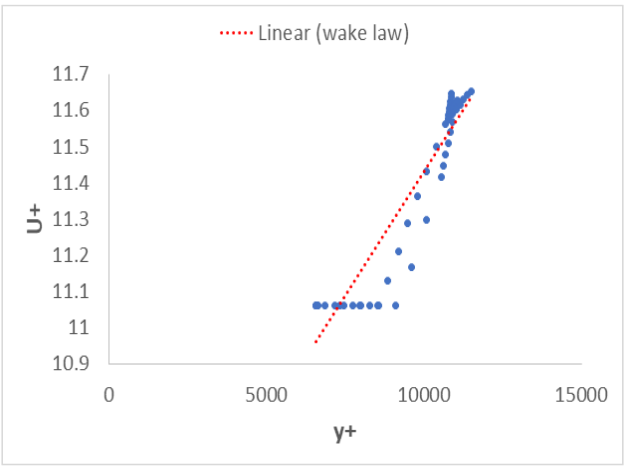

(2b)

Figure-2. (a) Illustration of fine mesh generated with COMSOL; (b) the variation of U^+ with respect to y^+ shows the outer layer/wake-law region of the boundary layer.

3. RESULTS AND DISCUSSIONS

3.1 Validation of Solution Method

The current work solved the Navier Stokes equations and the energy equation for forced convective transient turbulent flow using the finite element method. Turbulence was modelled using the standard k- ε model interface of COMSOL Multiphysics. In order to validate the software employed, simulation of convective flow over a single circular cylinder at Re_D = 100 was carried out. The results obtained for Re_D = 100 were compared with the set of benchmark results [23] as presented in Table-3. The present result has a good agreement with the benchmark, with only 0.67% discrepancy in the maximum drag coefficient.

Table-3. Drag coefficient, lift coefficient and Strouhal number, St about a single cylinders Re_D = 100.

Present work: COMSOL			**Schafer and Turek [23] Method: FE block structured Q1 (rot)- Q0 adaptive upwind**		
$C_{D\,max}$	$C_{L\,max}$	St	C_{Dmax}	C_{Lmax}	St
3.2096	0.92188	0.2174	3.2314	0.9999	0.2973

3.2 Heat Transfer Characteristics

The heat transfer patterns over the cylinders are shown by the means of isotherm contours, surface temperature plot, and Nusselt number plot. Figure-3 shows the heat transfer characteristics over the cylinders and downstream the flow domain.

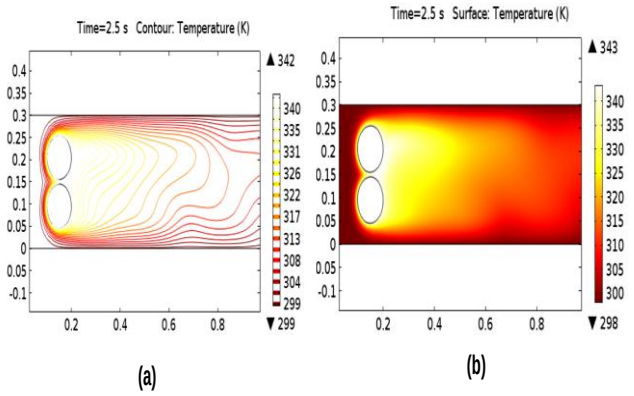

Figure-3. Heat transfer characteristics over the cylinders with S = 1.1D.

In Figur-3a, the isotherm contours are closely located to each other on the front of the cylinders. Behind and on other portions of the cylinders, the isotherms are more spaced than the front region. This implies that there is higher heat transfer characteristic at the front. A close look at the colour legend further explains this. The temperature (with deep yellow) on the front surface of the cylinders is highest. Due to fluid flow, temperature being referred to is the total temperature- a sum of the static temperature and dynamic temperature. The isotherms (red) representing surfaces away from the front of the cylinders indicate less temperature; it shows that heat is being transported essentially by the flow. Similar result is reported by [24] though their work was based on low Reynolds number. Figure 3b represents temperature field in the flow domain by colour shades. It highlights the same heat transfer characteristics pattern around the cylinders, and along the flow channel as shown earlier in Figure-3a. For smaller spacing ratio S = 1.1D as well as 1.3≤S/D ≤5, the isotherms are also more crowded on the front of the cylinders than the top, bottom and the rear parts. Figures 4 and 5 show the isotherms and surface temperature plot over the cylinders for S/D = 2 and 2.4 respectively. Similarly, more isothermal contours of different values are crowded on the front parts of the cylinders as shown in Figures 4a and 5a. Figures 4b and 5b also show that the temperature is high in the region of the cylinders, but reduces downstream. This also corroborates that heat is transported by the flow.

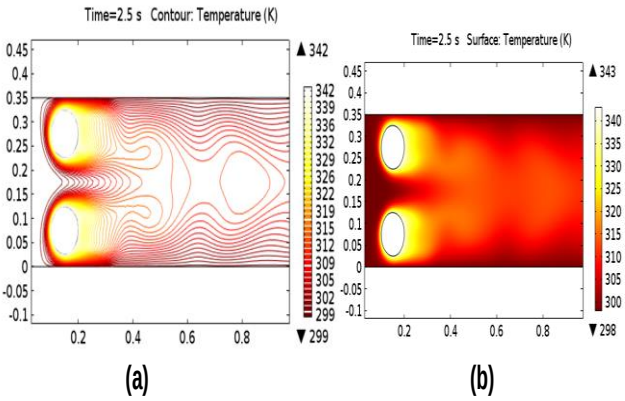

Figure-4. Isotherms (a) and surface temperature (b) for S = 2D.

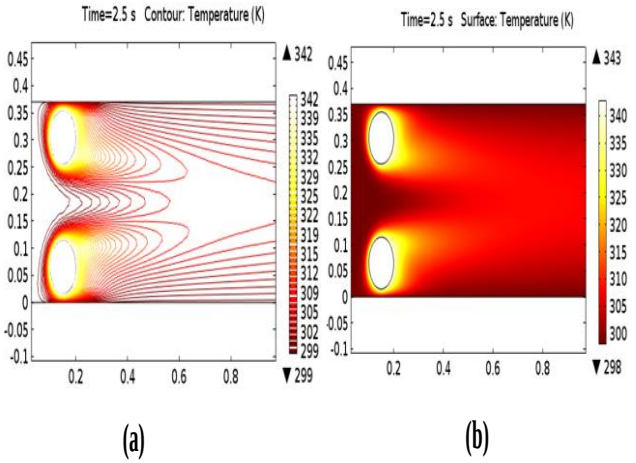

Figure-5. Isotherms (a) and surface temperature (b) for S = 2.4D.

Nusselt number, another heat transfer characteristic, is evaluated at front (just upstream), top, bottom and rear (just downstream) parts of each of the two cylinders, and the mean is determined. The mean surface Nusselt number plot shown in Figure-6 supports the observations presented by Figures 3, 4 and 5. It shows that Nusselt number is highest at the front region or section of the cylinders compared to the top, bottom or rear parts. The mean Nusselt number of the surfaces of the cylinders generally decline as the spacing ratios increase. However, on the front surface the mean Nusselt number goes up for S/D = 5, while the declining pattern of Nusselt number for the rear surface occurs for 2≤S/D≤5 as shown in Figure-6. The variation of the mean Nusselt number of the entire cylinders with the S/D ratios is presented in Figure-7, and it shows that mean Nusselt number decreases as the S/D ratio increases. It is noted from Figures 6 and 7 that the variation of Nusselt number with the S/D is continuous, so that the parameter can be invested at any discrete spacing ratio within the critical range 1≤ S/D≤5.

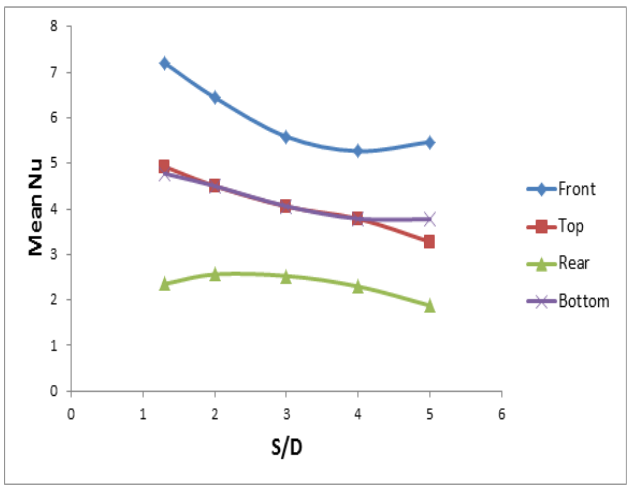

Figure-6. Variation of mean Nusselt number of the four portions of the two cylinders.

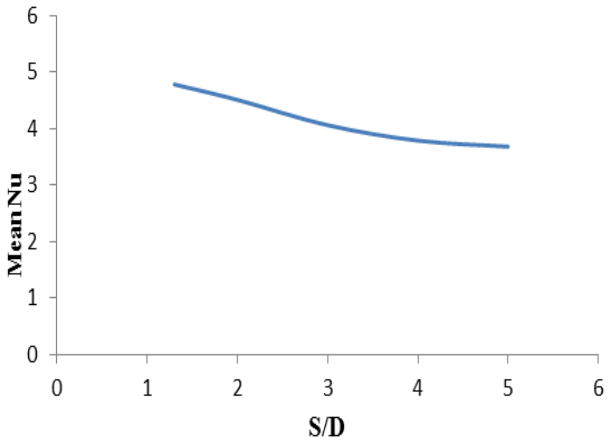

Figure-7. Variation of mean Nusselt number of the two cylinders with S/D.

3.3 Vortex Structure and Flow Pattern

Figure-8 illustrates vortex structure, vortex shedding and streamline over the cylinders. The wake interactions behind and between the cylinders are shown in Figure-8a for S/D = 1.3. At this small spacing ratio, there is considerable wake behind the cylinders. The vortex structures are clearly visible, but tiny and possess in-phase synchronized pattern. The shedding at the top part of the upper cylinder is in synchronization with the shedding taking place at the top part of the lower cylinder. This is also true for vortex shedding at the bottom parts of the cylinders. Figure-8c shows that vortex structures merge downstream the flow channel for S/D =1.1. For this spacing, the vortex structures are small and vortex shedding between the cylinders is strongly suppressed. This was also reported in [9, 25]. Over time, they spread laterally and form a single structure behind the cylinders, as shown in Figure-8c. This figure also shows that flow through the gap is completely dominated by jets. Jet flow, which is characterized with interference of wakes from and between the two cylinders as a result of the small gap [31], occurs at S/D <2.

For 2≤S/D ≤4, the vortex structures are visible and distinct throughout the flow domain, without spreading laterally. The vortex shedding from the upper and the lower cylinders are in anti-phase synchronization for S/D =3 (Figure-8b). The streamline plot (Figure-8d) shows that the flow is of symmetric pattern at S/D = 2, i.e., streamlines over each cylinder approximately mirrors those from the other cylinder. As the spacing increases (S/D ≥2), wake interaction between the cylinders gets weaker, and this is responsible for the distinct vortex structures that do not spread laterally. For S/D = 5, the wake interaction behind and between the cylinders is weakest. The flow interaction between and over the cylinders vanishes quickly.

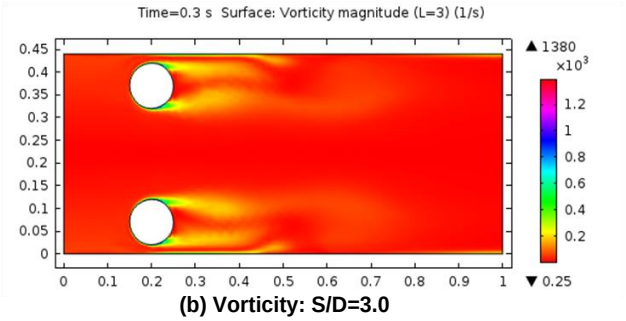

(b) Vorticity: S/D=3.0

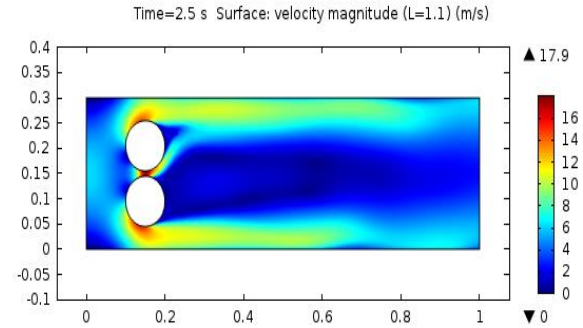

(c)Vortex shedding: S/D=1.1

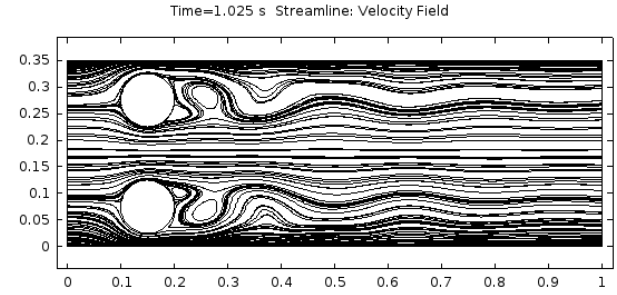

(d) Streamlines: S/D=2.0

Figure-8. Vortex structure and the streamlines at various ≥.

3.4 Lift and Drag Coefficient and the Strouhal Number

Figure-9 presents the histories of the lift coefficients and frequency spectrum over the cylinders. The lift coefficient fluctuations over the pair of cylinders at ≥=1.3 are shown in Figure-9a. The mean lift coefficient for S/D=1.3 at the lower cylinder is negative while the mean lift coefficient of the upper cylinder is positive. The Strouhal number is also obtained for the same spacing as shown in Figure-9d. Where a sharp peak is obtained, the frequency is called Strouhal frequency, a measure of the Strouhal number. This value indicates high unsteadiness and high frequency of vortex shedding around the lower and upper cylinders. The mean drag coefficients for the lower and upper cylinders are both positive.

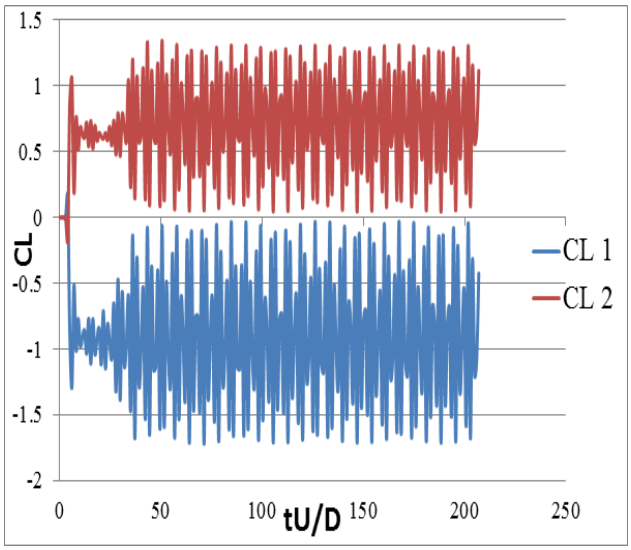

(a) S/D=1.3

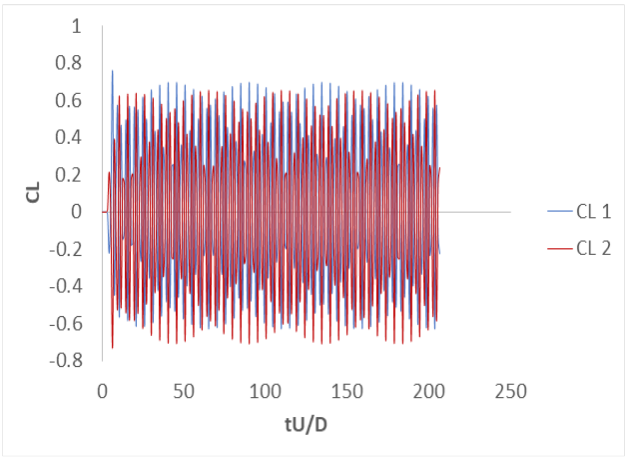

(b) S/D = 2

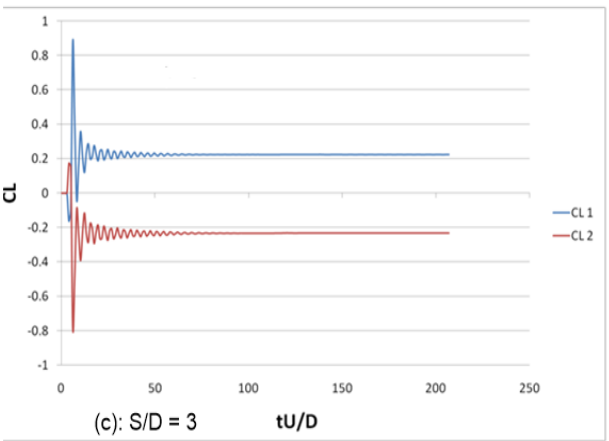

(c): S/D = 3

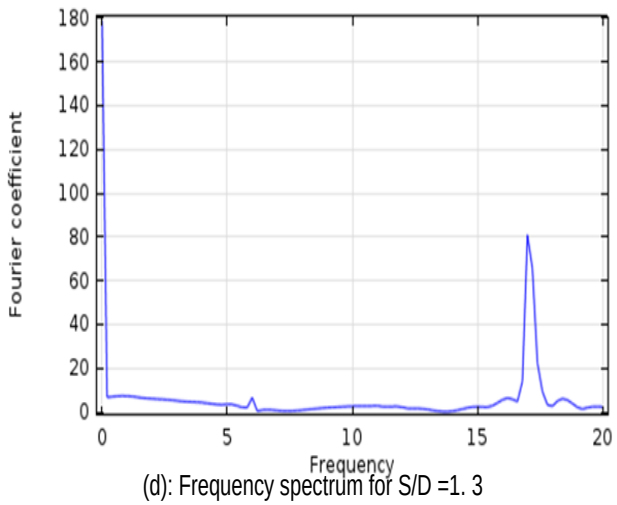

Figure-9. The oscillation of the Lift coefficient for various S/D (a) 1.3; (b) 2; (c) 3 and Frequency spectrum for S/D = 1.3 (d) explains the peak at which Strouhal frequency- a measure of Strouhal number is obtained. Subscript 1 indicates lower cylinder while subscript 2 represents upper cylinder.

The lift coefficients for S/D = 2 (Figure-9b) over the two cylinders shows flip-flop pattern which is biased; this means that the flow switches in opposite direction from one cylinder to the other. The lift coefficient of the upper cylinder is negative while that of the lower cylinder is positive. At S/D = 3, the mean values of the lift coefficient variations over the cylinders are equal but opposite and the amplitudes decayed over time (Figure-9c). Figures 9c and 8b show that lift coefficients about the cylinders are therefore in anti-phase synchronized pattern. The mean drag coefficients are the same for the upper and lower cylinders as shown in Figure-10. Figure-10 shows fluctuation of the drag coefficient over time. It shows that there are similar trends in the drag coefficient variations of the upper and lower cylinders. For other spacing ratios, the lift coefficient, drag coefficient and Strouhal Number are presented in Table-4. Table-4 presents the lift coefficient, drag coefficient and Strouhal number at Re_D = 23 500. It shows that as spacing ratio increases, the mean drag coefficient decreases.

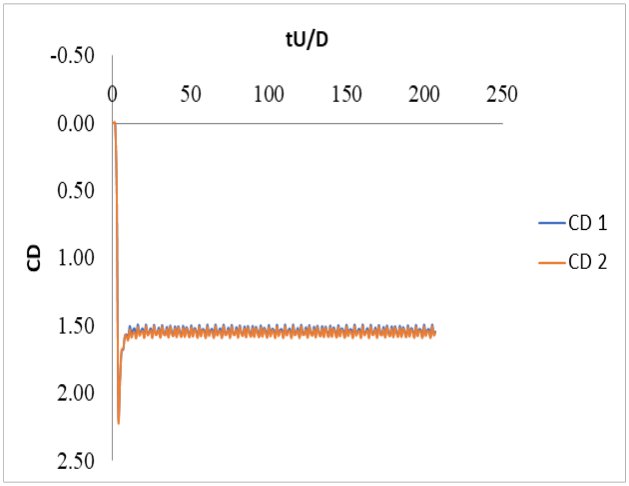

Figure-10. Time history of the drag coefficient for S/D = 2.

Table-4. Summary of the lift, drag coefficient and Strouhal number at Re_D= 23500.

Spacing Ratios (S/D)		Mean Lift Coefficient (C_L)	Mean Drag Coefficient (C_D)	Strouhal Number (St)
1.1	UC	0.79	4.58	-
	LC	-3.18	3.79	-
1.3	UC	0.69	3.08	0.4107
	LC	-0.89	3.08	0.4107
2.0	UC	-0.026	1.53	0.382
	LC	0.034	1.53	0.382
3.0	UC	-0.22	1.17	-
	LC	0.22	1.17	-
4.0	UC	-0.14	0.74	0.256
	LC	0.14	0.74	0.256
5.0	UC	0.07	0.55	-
	LC	-0.15	0.55	-

UC refers to the upper cylinder while LC means lower cylinder

4. CONCLUSIONS

The flow parameters and heat transfer characteristics at different spacing ratios over a pair of circular cylinders at Re_D = 23500 were determined. The following deductions are made from a set of numerical simulations conducted at S/D = 1.1, 1.3, 2.0, 2.4, 3.0, 4.0 and 5.0 for side-by-side arrangement of the two circular cylinders in a confined rectangular channel by solving continuity, momentum and energy equations using finite-element based software (COMSOL Multiphysics):

a) The heat transfer characteristics, measured by Nusselt number as well as depicted by isotherms and temperature field, are higher at the front parts of the two cylinders than the top, rear and bottom portions. The flow process is responsible for the transport of heat downstream.
b) The mean Nusselt number of the parts (front, top, rear and bottom) of the cylinders decreases as the S/D ratio increases. The inverse relationship between the mean Nusselt number and the spacing ratio is true for the rear portion within the limit $2 \leq S/D \leq 5$. For the frontal surface of the cylinders, the mean Nusselt number rather increases at S/D = 5. Generally, the mean Nusselt number of the cylinders entirely declines with increase in the S/D ratios.
c) There is strong wake interaction between the cylinders at small spacing ratios. At spacing ratio below 2, the vortex structures spread laterally and merge behind the cylinders. At S/D = 1.1, the vortices behind the cylinders quickly merge. The small gap is completely dominated by jets, where the flow downstream is vigorous and chaotic. For S/D = 2, the flow pattern is symmetric. For $S/D \geq 2$, the flow interaction gets weaker, and the vortex structures are distinct and do not spread laterally. For S/D = 5, the flow interaction is very weak and vanishes quickly.
d) The lift coefficient at S/D = 2 over the two cylinders has a biased flip-flop pattern. The mean drag coefficients of the cylinders for this spacing ratio are the same. For spacing ratio S/D = 3, the lift coefficient over the cylinders fluctuates in anti-phase synchronised pattern. As spacing ratio increases, the mean drag coefficient decreases.

NOMENCLATURE

q'' is heat flux.
q''' is heat generation per unit volume.
C_D is drag coefficient; C_L is lift coefficient.
D is diameter of the cylinder.
h_θ is local convective heat transfer coefficient.
K is thermal conductivity of the fluid.
S/D is centre-to-centre spacing to diameter ratio.
$Nu_\theta$is local Nusselt number.
P is pressure.
Re is Reynolds number and Re_D is the Reynolds number based on diameter.
S_{ij} is strain deformation.
S is centre-to-centre distance between the two cylinders
T is temperature.
T_w is the temperature at the cylinder wall
T_m is the bulk temperature of the fluid.
U_∞ is free stream velocity.
V means velocity.
δ_{ij}means kronecker delta.
μ_t is the turbulent (eddy) viscosity.
μ is molecular dynamic viscosity
ρ is density.
ε is the rate of dissipation of kinetic energy
k is the turbulent kinetic energy.
Pr is Prandtl number.

REFERENCES

[1] Zdravkovich M. M.: Review of flow interference between two circular cylinders in various arrangements. American Society of Mechanical Engineers, Journal of Fluids Engineering, Vol. 99, pp. 618-633, 1977.

[2] Suzuki K, Suzuki H.: Unsteady heat transfer in a channel obstructed by an immersed body. Annual Review of Heat Transfer, Vol. 5, pp. 177-206, 1994.

[3] Valencia A. 1996. Unsteady flow and heat transfer in channel with a built-in tandem of rectangular cylinders part a. Numerical Heat Transfer, Vol. 29, pp. 613-623, 1996.

[4] Moffat R. J., Ortega A. 1988. Direct air cooling of electronic components. Advances in Thermal Modelling of Elecronic Components and Systems, Eds. Bar-Cohen and A. Kraus. New York: Hemisphere. Vol. 1.

[5] Cengel Y. A., Cimbala J. M. 2006. Fluid mehanics: Fundamentals and applications, 1st ed. Boston: McGraw-Hill Higher Education.

[6] Sarvghad-Moghaddam H., Nooredin N., Ghadiri-Dehkordi B. 2011. Numerical simulation of flow over two side-by-side circular cylinders. Journal of Hydrodynamics. 23(6): 792-805.

[7] Kang S. 2003. Characteristics of flow over two circular cylinders in a side-by-side arrangement at low Reynolds numbers. Journal of Physics of Fluids. 15(9): 2486-2498.

[8] Chen W., Ji C., Xu W., Liu S., Campbell J. 2015. Response and wake patterns of two side-by-side elastically supported circular cylinders in uniform laminar cross-flow. Journal of Fluids and Structures. 55: 218-236.

[9] Williamson C. H. K. 1985. Evolution of a single wake behind a pair of bluff bodies. Journal of Fluid Mechanics. 159: 1-18, 1985.

[10] Bearmann, P. W., Wadcock A. J. 1973. The interaction between a pair of circular cylinders normal to a stream. Journal of Fluid Mechanics. 61: 499-511.

[11] Meneghini, J. R. and Saltara F. 2001. Numerical simulation of flow intereference between two circular cylinders in tandem and side-by-side arrangements. Journal of Fluids and Structures. 15: 327-350.

[12] Sumner D., Wong S. S. T., Price S. J., Paidoussis M. P. 1999. Fluid behaviour of side-by-side circular cylinders in steady cross-flow. Journal of Fluids and Structures. 13: 309-338.

[13] Bao Y., Zhou D., Tu J. 2013. Flow characteristics of two in-phase oscillating cylinders in side-by-side arrangement. Computers and Fluids. 71: 124-145.

[14] Lee D. S., Ha M. Y., Yoon H. S, Balachandar S. A. 2009. Numerical study on the flow patterns of two oscillating cylinders. Journal of Fluids and Structures. 25: 263-283.

[15] Golani R., Dhiman A. K., 2014. Fluid and heat transfer across a circular cylinder in the unsteady regime. The International Journal of Engineering and Science. 3(3): 08-19.

[16] Yoon H. S., Seo J. H., Kim J. H. 2010. Laminar forced convection heat transfer around two rotating side-by-side circular cylinders. International Journal of Heat and Mass Transfer. 53: 4525-4535.

[17] Chaitanya N. S. K., Dhiman A. K. 2012. Non-Newtonian power-law flow and heat transfer across a pair of side-by-side circular cylinders. International Journal of Heat and Mass Trassfer. 55: 5941-5958.

[18] Dos-Santos E. D., Da Silva F. M. V., Acunha I. C Jr., Galarca M. M., Isoldi, L. A., Rocha L. A. 2012. Numerical investigation of turbulent forced convective flows over a pair of circular cylinders. Thermal Engineering. 11(1): 77-84.

[19] Versteeg H. K., Malalasekera W. 2007. An Introduction to Computational Fluid Dynamics: the finite volume method, Pearson Education Limited.

[20] Hoffmann K. A., Chiang S. T.: Computational fluid dynamics, Kansas: Engineering Education System. 2000.

[21] Lienhard J. H. 2006. A heat transfer textbook, 3rd ed. Massachusetts Phlogiston Press.

[22] COMSOL: 2014. multiphysics reference manual. COMSOL.

[23] Schafer M., Turek S. 1996. Benchmark computations of laminar flow around a cylinder. Ed. Hirschel E. H. Flow simulation with high-performance computers ii. Notes on Numerical Fluid Mechanics Vieweg. 52: 547-566.

[24] Chatterjee D., Biswas G., Amiroudine S. 2009. Numerical investigation of forced convective heat transfer in unsteady flow past a row of square cylinders. International Journal of Heat and Fluid Flow. 30: 1114-1128.

[25] Bearmann P. W., Zdravkovich M. M. 1978. Flow around a circular cylinder near a plane boundary. Journal of Fluid Mechanics. 89(1): 33-47.

[26] Yang F. 2009. Slip boundary condition for viscous flow over solid surfaces, Chemical Engineering Communications. 197(4): 544-550.

[27] Moukalled F., Mangani L., Darwish, M. 2016. Implementation of boundary conditions in the finite-volume pressure-based method-Part I. Segregated solvers, Numerical Heat Transfer, Part B: Fundamentals. 69(6): 534-562.

[28] Tu J., Yeoh G. H., Liu C. 2008. Computational Fluid Dynamics A Practical Approach, Butterworth-Heinemann, Elsevier.

[29] [Molina-Aiz F. D., Fatnassi H., Boulard T., Roy J. C. Valera D. L. 2010. Comparison of finite element and finite volume methods for simulation of natural ventilation in greenhouses, Computers and Electronics in Agriculture. 72: 69-86.

[30] Rodriguez S. 2019. Applied Computational Fluid Dynamics and Turbulence Modeling Practical Tools, Tips and Techniques, Springer.

[31] Lam K, Li J. Y., So R. M. C. 2003. Force Coefficients and Strouhal Numbers of Four Cylinders in Cross Flow. Journal of fluids and structures. 18: 305-324.